

Domain-wall superconductivity in superconductor–ferromagnet hybrids

ZHAORONG YANG¹, MARTIN LANGE¹, ALEXANDER VOLODIN², RITTA SZYMCZAK³
AND VICTOR V. MOSHCHALOV^{1*}

¹Nanoscale Superconductivity and Magnetism Group, ²Scanning Probe Microscopy Group, Laboratory for Solid State Physics and Magnetism, K. U. Leuven, Celestijnenlaan 200D, B-3001 Leuven, Belgium

³Polish Academy of Sciences, Institute of Physics, al. Lotnikow 32/46, Warszawa 02-668, Poland

*e-mail: Victor.Moshchalkov@fys.kuleuven.ac.be

Published online 3 October 2004; doi:10.1038/nmat1222

Superconductivity and magnetism are two antagonistic cooperative phenomena, and the intriguing problem of their coexistence has been studied for several decades. Recently, artificial hybrid superconductor–ferromagnet systems have been commonly used as model systems to reveal the interplay between competing superconducting and magnetic order parameters, and to verify the existence of new physical phenomena, including the predicted domain-wall superconductivity (DWS). Here we report the experimental observation of DWS in superconductor–ferromagnet hybrids using a niobium film on a BaFe₁₂O₁₉ single crystal. We found that the critical temperature T_c of the superconductivity nucleation in niobium increases with increasing field until it reaches the saturation field of BaFe₁₂O₁₉. In accordance with the field-shift of the maximum value of T_c , pronounced hysteresis effects have been found in resistive transitions. We argue that the compensation of the applied field by the stray fields of the magnetic domains as well as the change in the domain structure is responsible for the appearance of the DWS and the coexistence of superconductivity and magnetism in the superconductor–ferromagnet hybrids.

The interaction between superconductivity and magnetism has been intensively studied^{1,2}. Recently, hybrid superconductor–ferromagnet (S/F) systems have attracted considerable attention because it is believed that the interaction between superconducting and magnetic-order parameters at the mesoscopic length scale may lead to new physical phenomena^{3–15}. In the S/F hybrids, an inhomogeneous distribution of magnetic field produced by the ferromagnet can lead to a significant change in the superconducting properties of the S-layer, including its critical temperature T_c . Different ferromagnetic systems can be used in the S/F hybrids: individual magnetic dots^{12,13} or arrays of these¹⁴, and non-patterned ferromagnetic thin films with bubble domains¹⁵. Depending on the domain structure of the ferromagnet, theory^{3,4} predicts a non-trivial T – H phase diagram for the nucleation of superconductivity in an external applied magnetic field H . Here we study superconductivity in S/F hybrids by using well-characterized single-crystal BaFe₁₂O₁₉ as a ferromagnetic sub-system. The basic idea is illustrated in the right-hand panels of Fig. 1: a superconducting Nb film (S) is placed on top of the ferromagnetic substrate (F) with the easy axis of magnetization in the z direction. In this case the stray fields in the thin S-film can be considered as almost homogeneous over the domain. On decreasing the temperature, superconductivity in zero applied field, $H_a = 0$, must first appear in the thin film just above the domain wall of the substrate (dark blue colour in Fig. 1b) because in that area the stray fields are the lowest¹⁶. An application of an external magnetic field results in a partial or complete compensation of the stray field above the reversed domains and makes it favourable for the superconductivity to nucleate in the place corresponding to the minimum of the total magnetic field. In other words, it is highly favourable for superconductivity to nucleate above domains of the opposite polarity in this case (see dark blue areas in Fig. 1a,c).

To implement this idea, we deposited a 50 nm Nb film by molecular beam epitaxy on a single-crystal BaFe₁₂O₁₉ (0001) substrate ($420 \times 420 \times 90 \mu\text{m}^3$) with 10-nm Si as a buffer layer between Nb and BaFe₁₂O₁₉. X-ray diffraction studies show that Nb film on Si has the (110) texture. Analysis by atomic force microscopy reveals that the r.m.s. roughness of the Nb film is about 2 nm over an area of $1 \mu\text{m}^2$.

Hexagonal BaFe₁₂O₁₉ is a well-known ferrimagnet with a uniaxial anisotropy lying along its [0001] direction. Figure 2 shows normalized magnetization loops of the BaFe₁₂O₁₉ (0001) substrate (measured in a Physical Properties Measurement System; Quantum Design). The normalized $M(H)$ curve taken at 5 K

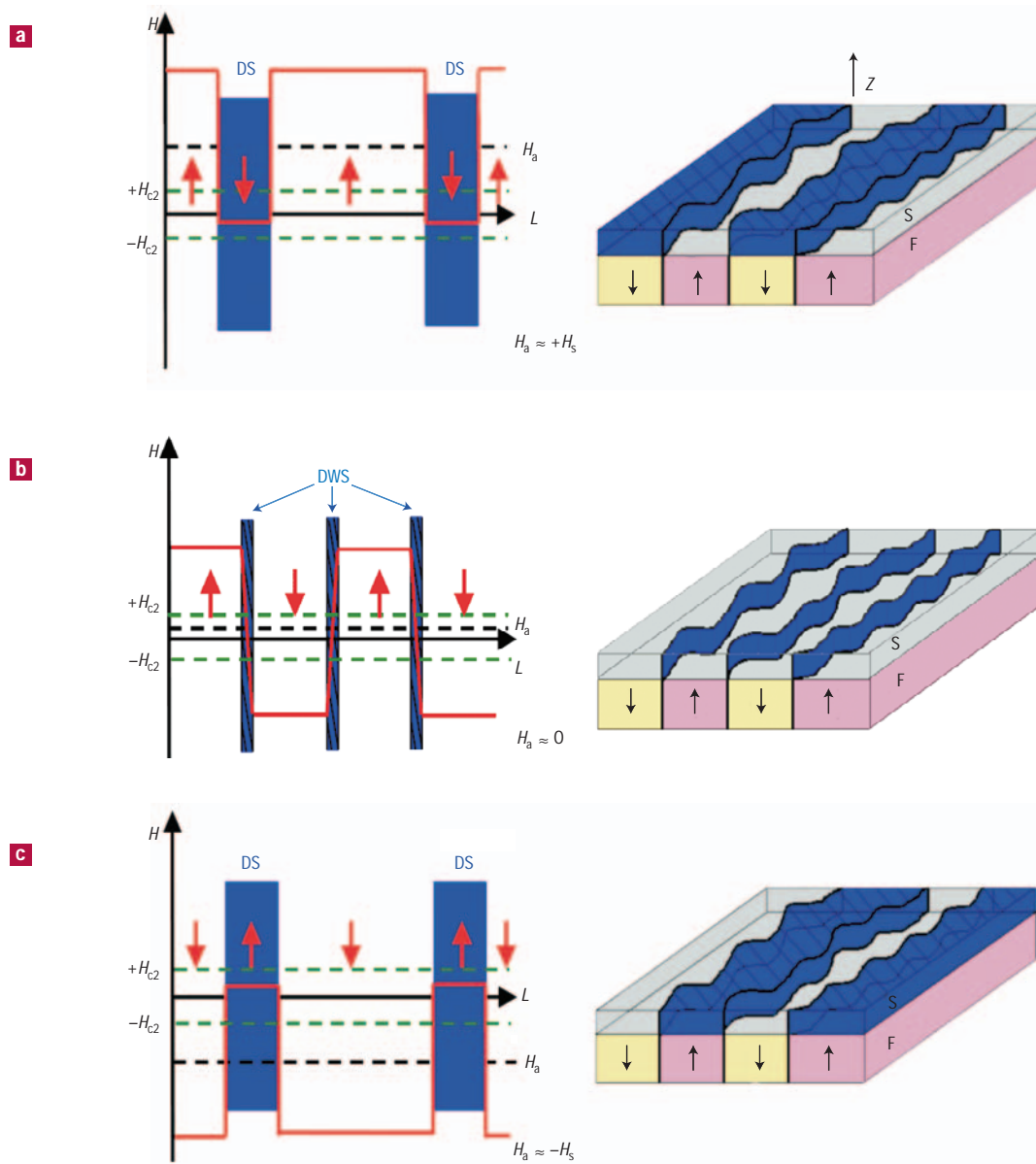


Figure 1 Schematic illustrations of domain-wall superconductivity (DWS) in superconductor–ferromagnet hybrids. Left, the magnetic field distribution in the superconducting layer at different applied magnetic fields H_a : **a**, $H_a \approx +H_s$, **b**, $H_a \approx 0$, and **c**, $H_a \approx -H_s$, where H_s is the saturation field. DS denotes domain superconductivity, and L is distance in the plane of the thin film. Black dashed horizontal lines indicate the applied field H_a . Green dashed lines indicate the upper critical field H_{c2} . Red solid lines show the total magnetic field, $\vec{H}_a + \vec{H}_q$. Right, schematic images of the superconducting areas (dark blue) in the superconductor–ferromagnet hybrid structure. F denotes ferromagnet with easy axis in the z direction and with thickness much larger than the distance between domain walls. S stands for the superconducting Nb thin film. Dark arrows show the orientation of the magnetic moment in the magnetic domains.

almost coincides with that taken at 300 K. Both have very similar behaviour. From zero field up to almost the saturation field, these loops are closed. Around the saturation field, however, hysteresis is clearly visible for both temperatures, as shown in the insets to Fig. 2. From the similarity between these two curves, we can expect that the domain structure of $\text{BaFe}_{12}\text{O}_{19}$ is very similar at 5 K and at 300 K.

The microscopic domain structure of the $\text{BaFe}_{12}\text{O}_{19}$ (0001) substrate has been investigated by magnetic force microscopy (MFM) at room temperature using a commercial Autoprobe M5 scanning probe microscope (VEECO Instruments) in ‘flying’ mode. A mechanically adjusted permanent magnet providing uniform

fields up to 5 kOe was mounted to study the evolution of the domain structure with field. The MFM images (Fig. 3) were recorded by ramping the field from remanent state towards saturation and back again along the major hysteresis loop. In the remanent state, the MFM image displays a branched domain pattern with a domain width of about 1.9 μm . Very similar patterns for $\text{BaFe}_{12}\text{O}_{19}$ have been reported previously¹⁷. This kind of domain pattern exists because of domain branching and is typical for materials with uniaxial anisotropy^{18,19}. In the first approximation, dark yellow and red regions can be attributed to magnetic domains with up and down magnetization, respectively. The width of the domain walls is about 200 nm.

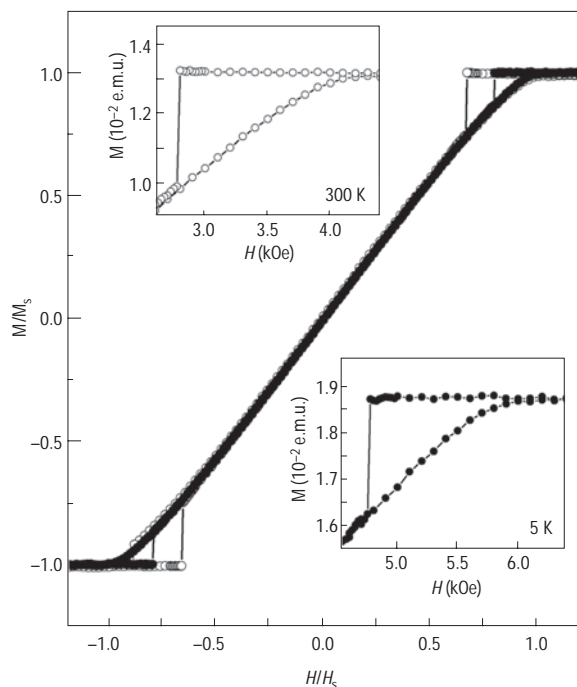


Figure 2 Magnetization versus applied magnetic field for the BaFe₁₂O₁₉ single-crystal substrate. The curves are normalized to the saturation field H_s and the saturation magnetization M_s . The main panel shows the normalized magnetization loops for the BaFe₁₂O₁₉ substrate with magnetic field along [0001] at 5 K and 300 K (filled and open circles, respectively). The insets are enlarged views of the magnetization loops around the saturation field at 5 K and 300 K.

With increasing field, the dark yellow area increase is accompanied by the growth of domains with positive magnetization, and the domain pattern becomes less branched. At 1.88 kOe elongated domains coexist with interstitial, isolated domains. The domain structure disappears completely at a saturation field of about 3.54 kOe. When the field is ramped down after the saturation, reversed domains start to nucleate at 2.99 kOe. The evolution of the domain structure displays clear hysteresis around the saturation field, in agreement with the magnetization loop, $M(H)$ (Fig. 2, inset). No evident hysteresis is observed at low fields, suggesting that the domain walls move freely in response to the variation of the external field²⁰.

We measured the resistance R of the Nb film deposited on BaFe₁₂O₁₉ in a Physical Properties Measurement System (Quantum Design) applying a four-probe a.c. technique with an alternating current of 10 μ A at a frequency of 19 Hz (Fig. 4). The distance between the voltage contacts amounts to 250 μ m. The magnetic field H is applied perpendicular to the sample surface from -15 kOe to $+15$ kOe. As seen from Fig. 4, the S/F structure shows a substantial broadening of the resistive superconducting transition even at zero field. At fields below 6 kOe, $R(T)$ curves cross each other. In contrast, the $R(T)$ curve for a reference sample has a sharp superconducting transition, and as expected, T_c shifts monotonically to lower temperature as H is increased (Fig. 4, inset). By defining T_c with three different resistance criteria, we constructed magnetic-field-temperature (H - T) phase diagrams for Nb/BaFe₁₂O₁₉, as shown in Fig. 5. For the resistance criterion $R_{\text{crit}} = 0.9R_n$, where R_n is the normal state resistance, T_c increases with increasing field until $H \approx 5.25$ kOe, and the phase boundary is almost symmetric with respect to H except near the saturation field. On increasing the field further, T_c

decreases abruptly, and the $T_c(H)$ phase boundary crosses over into a conventional linear regime when $|H|$ is above 6 kOe.

This very unusual effect—the increase of T_c with increasing magnetic field—is in accordance with theoretical predictions of the $T_c(H)$ behaviour for domain-wall superconductivity^{3,4}. To apply this model to the present system, the domain structure and its changes with H should be further considered. In our case, the domain-wall width (around 200 nm) is much larger than the coherence length of the Nb thin film $\xi(T)$ at $T = 7.84$ K (about 40.4 nm; see below). As the temperature is decreased at zero applied field, it is more favourable for superconductivity to nucleate above the domain wall owing to the lower stray fields at that location¹⁶. The overlap of the superconducting areas above different domain walls can be excluded in our experiments, because of the much larger domain size ($w \approx 1.9$ μ m is much greater than ξ). The present system corresponds well to the limit of isolated domain-wall superconductivity (the critical parameter $\pi H_d w^2 / \Phi_0 \approx 3,000 \gg 1$, where H_d is the maximum absolute value of the stray field above the magnetic domain, in our case ~ 5.4 kOe, w is the domain size, and Φ_0 is the superconducting flux quantum; see ref. 3).

The phase boundary for isolated domain-wall superconductivity is predicted to behave as³:

$$T_c(h) = \Delta T_c^{\text{orb}} (\frac{1}{2} - E_{\text{min}}) h^4 + \Delta T_c^{\text{orb}} (2E_{\text{min}} - \frac{1}{2}) h^2 + T_c(0) \quad (1)$$

where $h = H_a/H_d$ (with H_a an external applied magnetic field and $H_d \approx 4\pi \times$ saturation magnetization, M_s ; superscript ‘orb’ stands for orbital suppression of T_c). To deduce this formula, the authors assumed that the width of a domain wall is much less than the superconducting coherence length. Thus the distribution of magnetic field near the surface was taken as $H = 4\pi M_s \text{sgn}(x) + H_a$. With this assumption, the nucleation of superconductivity at zero field is analogous to surface superconductivity below the surface critical field H_{c3} , which gives a parameter $E_{\text{min}} = 0.59$. In the case of the BaFe₁₂O₁₉ single crystal, the stray field changes smoothly over the domain wall, so that the assumption of infinitely thin domain walls is no longer justified and the comparison with surface superconductivity is no longer valid. As a result, we can expect that E_{min} will deviate from 0.59. Fitting the experimental phase boundary by using equation (1) with E_{min} as the only variable parameter, we find that with $E_{\text{min}} = 0.37$ the experimental data are in good agreement with the theoretical model. Although equation (1), strictly speaking, was derived for domain-wall width less than $\xi(T)$, the good fit displayed in the inset of Fig. 5 suggests that DWS in Nb/BaFe₁₂O₁₉ can still be described by that model. We therefore hope that our results will stimulate further theoretical investigation in this field, in particular addressing the issue of the behaviour of $T_c(H)$ in the case of a broader domain wall.

The appearance of these localized superconducting nuclei results in a broadening of the superconducting transition as observed in the $R(T)$ curves (Fig. 4). The onset of the resistance decrease with temperature corresponds to the appearance of the DWS, and the crossover to the linear $T_c(H)$ behaviour signals the presence of the bulk superconductivity. As we increase the applied field the superconducting areas shift away from the domain walls towards the regions where the absolute value of the total magnetic field is minimal because of the compensation effects³. On the other hand, with increasing field, the domains with positive magnetization grow, accompanying the motion of the domain walls.

To understand the evolution of superconductivity with magnetic field at different fixed temperatures (Fig. 6), we shall first have a closer look at the variation of the local field across different magnetic domains (left panels in Fig. 1). After a magnetic field $H > +H_s$ has been applied, all domains are magnetized along the field \vec{H}_a . At fields slightly below $+H_s$, the first domains of negative polarity will appear (if the difference between the nucleation field and H_s

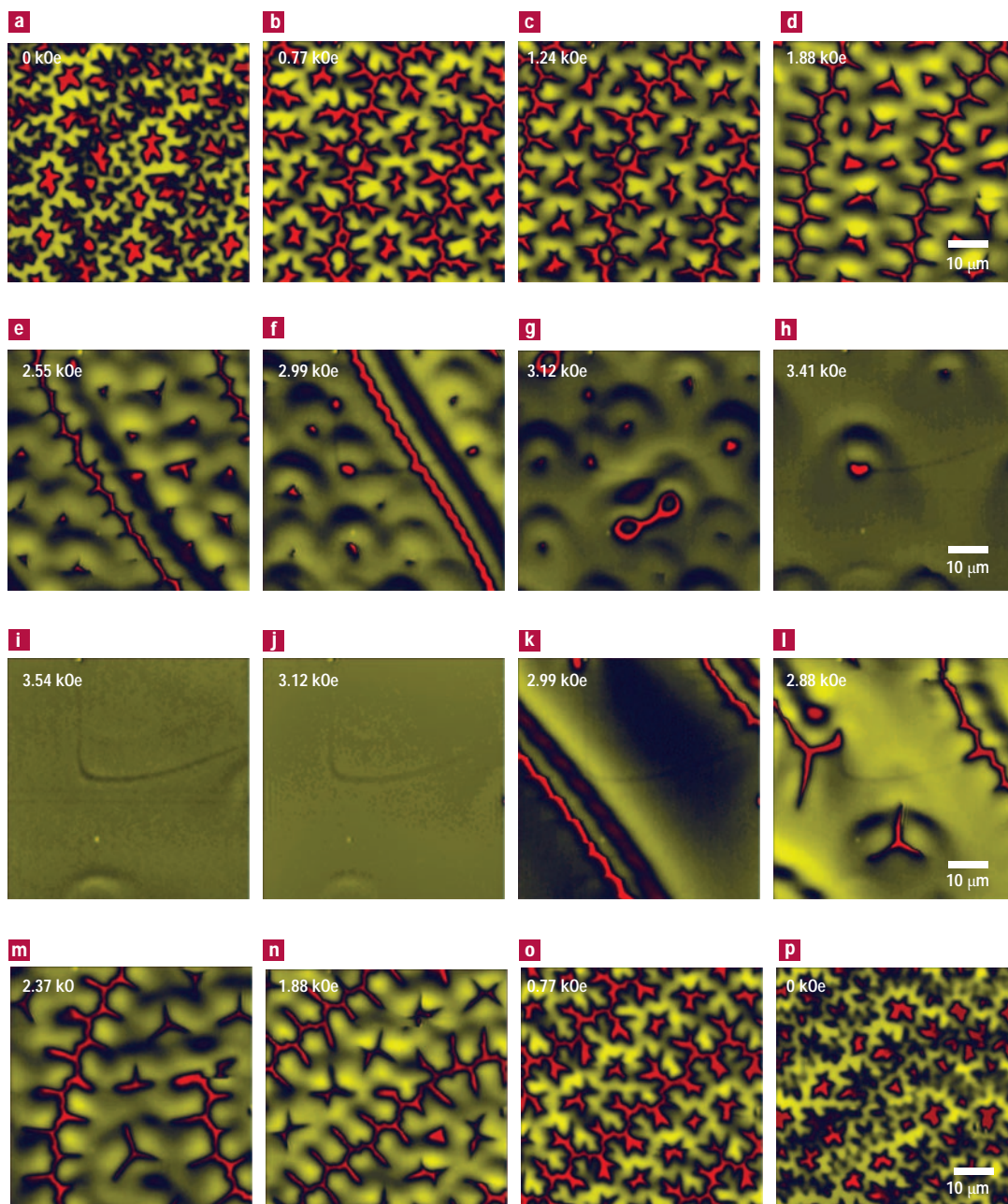


Figure 3 A series of MFM images for the BaFe₁₂O₁₉ (0001) substrate measured at room temperature with magnetic field applied perpendicular to the basal plane. The images cover 60 × 60 μm². In the remanent state (a), the MFM image displays a branched domain pattern. When a field is applied, the dark yellow area increases, signalling the growth of domains with +H_s magnetization. At the same time, the domain pattern becomes less branched. At 1.24 kOe (c), one can clearly see three branched stripe domains as well as several disjunct dendritic domains. As a consequence of a weaker branching with increasing field, the branched stripe domains and disjunct dendritic domains transform into straight lines and isolated bubbles (f), respectively. At 3.12 kOe (g), only the bubble domains can be observed. Above 3.54 kOe (i), the contrast is almost homogeneous, signalling the magnetic saturation of the sample. The line and dots displayed in i and j are due to the topography and dust particles. When the field is reduced from saturation, the evolution of the domain structure displays hysteresis around the saturation field H_s, which is in agreement with the M(H) loop shown in Fig. 2. Line-shaped reversed domains begin to nucleate at 2.99 kOe (k). After the field is ramped further down, disjunct dendritic domains nucleate and domain patterns display the branched structure again. At low fields, the domain pattern is almost identical to that taken by ramping the field from the remnant state towards saturation.

is ignored). Their local fields H_d are opposite to the applied field, and the |H_d| value is close to +H_s. These domains will practically completely compensate the applied field, |H_a - H_d| ≈ 0. As a result, superconductivity will appear in the areas just above domains of the opposite polarity in the ferromagnet (see domain superconductivity

areas in Fig. 1a; the red solid line shows the variation of the total field $\vec{H}_t = \vec{H}_a + \vec{H}_d$).

As the field is ramped down towards zero, the difference in amplitudes between |H_d| ≈ |H_s| and |H_a| grows and the compensation effect becomes less efficient above the domains themselves.

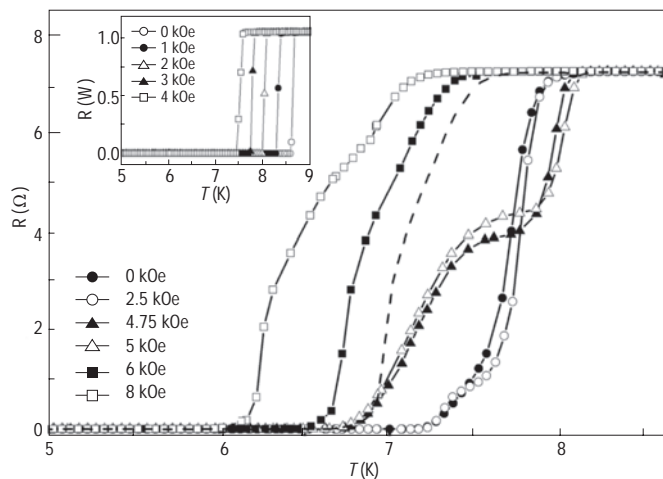


Figure 4 Temperature dependence of resistance R for Nb/BaFe₁₂O₁₉ in the field range 0 to 10 kOe. The field is ramped from -15 kOe to $+15$ kOe. The measured $R(T)$ curves depend on magnetic history. For example, at a field of 5 kOe, the superconducting transition will be at lower temperature if the field is ramped in the opposite direction, from 15 kOe to -15 kOe (dashed line). The inset shows the temperature dependence of R for a reference sample (50 nm Nb deposited on Si/SiO₂ substrate with 10 nm Si as buffer layer between Nb and SiO₂).

Remarkably, in the area of the domain wall the stray fields are substantially lower and there a weak field compensation effect is still possible (Fig. 1b, $H_a \approx 0$).

For negative applied fields the domain superconductivity will appear again near $H_a \approx -H_s$ (Fig. 1c). On the way from $H_a \approx 0$ to $H_a \approx -H_s$ the superconducting area, which was first located only at the domain walls, progressively captures the whole of domains with polarity opposite to that of the applied field. In other words, at $H_a \approx 0$ superconductivity survives only above the domain walls which define the boundaries of magnetic domains (see Fig. 1b, right). As the field is ramped up towards $+H_s$, or down towards $-H_s$, superconductivity spreads from the circumference of the domain to the whole domain area, provided that the latter has polarity opposite to that of the applied field (Fig. 1a and c, right panels). This remarkable transformation of the superconducting area with the applied field is responsible for the appearance of the two minima in the $R(H, T_0)$ curves—at $H \approx -H_s$ and $H \approx +H_s$ (see Fig. 6b). When temperature T_0 increases, the upper critical field H_{c2} of the superconducting film becomes so low that only the full field compensation above magnetic domains fulfils the constraint $||H_a| - |H_d|| < H_{c2}$. Because of that, the DWS is almost completely suppressed and superconductivity is still present only around $H \approx \pm H_s$ (see Fig. 6a). From the $R(H)$ curve measured at 8.15 K (not shown here), the value of H_d can be estimated to be about 5.4 kOe, where the resistance displays a minimum. This value is close to H_s for this temperature.

For a better understanding of the $R(H, T_0)$ curves, we have investigated the evolution of the domain structure of the BaFe₁₂O₁₉ substrate. Following the hysteretic domain evolution, when the field is swept up and down, a hysteresis also appears in the $R(H)$ curves, and the magnitude of the resistance depends strongly on the direction of the field sweep. For instance, as the field is ramped down from saturation, domain superconductivity is suppressed at fields above the nucleation field of reversed domains (Fig. 6, red filled circles). At $H/H_s = 0.83$, the superconducting transition of the film consistently occurs at lower temperature if the field is coming from saturation (Fig. 4, dashed line). A direct correlation between

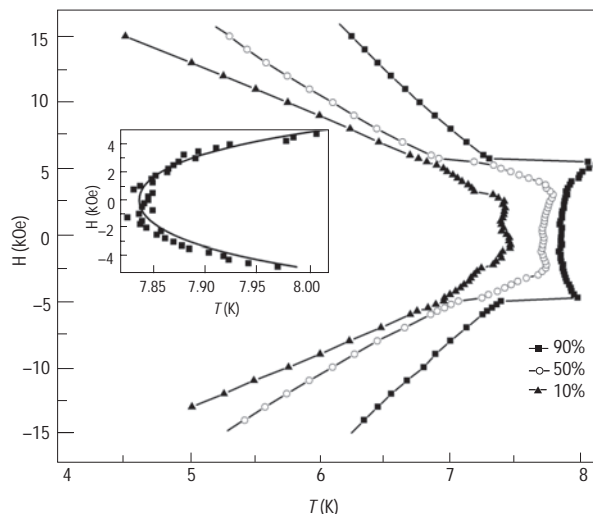


Figure 5 Superconducting phase diagram of Nb/BaFe₁₂O₁₉. The diagram was obtained from the $R(T)$ curves shown in Fig. 4 by defining the critical temperature with three different resistance criteria. The inset shows an enlarged view of the H – T phase diagram for the resistance criterion of $R_{\text{crit}} = 90\% R_n$. The solid line is a fit to equation (1) with fitting parameter $E_{\text{min}} = 0.37$. In the fitting, H_d is taken as 5.4 kOe corresponding to the field where $R(H)$ displays a minimum at 8.15 K and $T_c(0)$ is taken as 7.84 K. From the linear fitting for $|H| > 6$ kOe, we know that 5.4 kOe can shift the critical temperature by 0.6 K, $\Delta T_c^{\text{orb}} \sim 0.6$ K. For $|H| > 6$ kOe, the linear behaviour of the phase diagram can be fitted by $H_{c2}(T) = \Phi_0/2\pi\xi^2(T)$ with $\xi(0) = 6.67$ nm and $T_{c0} = 8.06$ K, where Φ_0 is the superconducting flux quantum, $\xi(T) = \xi(0)/(1 - T/T_{c0})^{1/2}$ the temperature-dependent coherence length in the dirty limit, and T_{c0} the critical temperature at zero total field ($\vec{H}_t = \vec{H}_a + \vec{H}_d = 0$). The coherence length at 7.84 K is about 40.4 nm.

hysteretic resistive transition and hysteretic domain evolution can be seen in Fig. 7. Here we compare the difference in the resistance for both field-sweep directions, $\Delta R = R(H_\downarrow) - R(H_\uparrow)$ (where H_\downarrow and H_\uparrow are the fields for a sweep down and up, respectively), with the difference in the reverse domain area at corresponding fields $\Delta f = f(H_\downarrow) - f(H_\uparrow)$. The area of reversed domains f was derived by image processing of the MFM data in Fig. 3. The good correlation between ΔR and Δf suggests that the hysteretic resistive transition does indeed result from the hysteretic domain evolution. Clearly the measured resistance not only depends on the compensation effect but also reflects the total area of the available reversed domains.

Our discovery of domain-wall superconductivity in Nb/BaFe₁₂O₁₉ hybrids, together with hysteretic resistive transitions and field compensation effects, makes it possible to control the superconducting order parameter at the nanoscale by tuning the domain structure in the ferromagnetic substrate. Using these systems is also promising for achieving vortex manipulation, with the help of controlled domain-wall motion, which will be important for the operation of fluxonics devices.

Received 8 March 2004; accepted 9 August 2004; published 3 October 2004.

References

- Flouquet, J. & Buzdin, A. Ferromagnetic superconductors. *Phys. World* **15**, 41–46 (2002).
- Bulaevskii, L. N., Buzdin, A. I., Kulić, M. L. & Panjukov, S. V. Coexistence of superconductivity and magnetism: theoretical predictions and experimental results. *Adv. Phys.* **34**, 175–261 (1985).
- Aladyshkin, A. Y. *et al.* Domain-wall superconductivity in hybrid superconductor–ferromagnet structures. *Phys. Rev. B* **68**, 184508 (2003).
- Buzdin, A. I. & Mel'nikov, A. S. Domain wall superconductivity in ferromagnetic superconductors. *Phys. Rev. B* **67**, 020503(R) (2003).

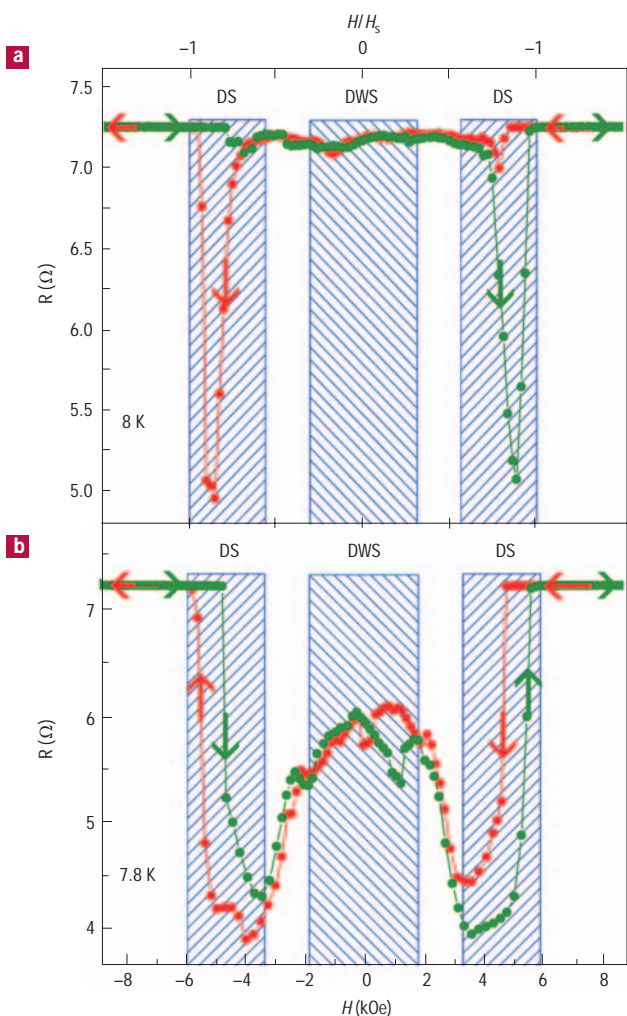


Figure 6 Field dependence of resistance of the Nb/BaFe₁₂O₁₉ hybrid system. **a**, At 8 K; **b**, at 7.8 K. The field is applied in the z direction. The field is first swept from 10 kOe to -10 kOe (red filled circles) and then back from -10 kOe to 10 kOe (dark green filled circles). The arrows indicate the field sweep direction. DS (domain superconductivity) and DWS (domain-wall superconductivity) indicate the different regimes for the nucleation of superconductivity.

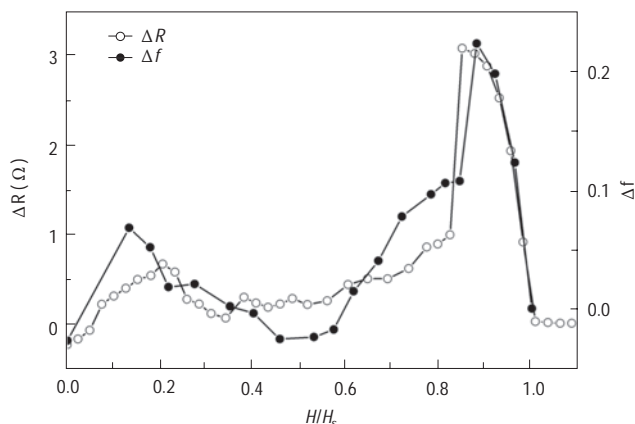


Figure 7 Comparison of hysteretic resistive transitions and hysteretic domain evolution. The data ΔR (open circles) show the difference in resistance (at $T = 7.8$ K) at corresponding fields, $\Delta R = R(H_{\downarrow}) - R(H_{\uparrow})$, and Δf (solid circles) denotes the difference in the reverse domain area at corresponding fields, $\Delta f = f(H_{\downarrow}) - f(H_{\uparrow})$. The parameter f was derived from the MFM data (Fig. 3) by dividing the red area (reversed domain) by the total area.

- Lyuksyutov, I. F. & Pokrovsky, V. L. Magnetization controlled superconductivity in a film with magnetic dots. *Phys. Rev. Lett.* **81**, 2344–2347 (1998).
- Erdin, S., Lyuksyutov, I. F., Pokrovsky, V. L. & Vinokur, V. M. Topological textures in a ferromagnet-superconductor bilayer. *Phys. Rev. Lett.* **88**, 017001 (2002).
- Martin, J. I., Vélaz, M., Nogués, J. & Schuller, I. K. Flux pinning in a superconductor by an array of submicrometer magnetic dots. *Phys. Rev. Lett.* **79**, 1929–1932 (1997).
- Bulaevskii, L. N., Chudnovsky, E. M. & Maley, M. P. Magnetic pinning in superconductor-ferromagnet multilayers. *Appl. Phys. Lett.* **76**, 2594–2596 (2000).
- Helseth, L. E., Goa, P. E., Hauglin, H., Baziljevich, M. & Johansen, T. H. Interaction between a magnetic domain wall and superconductor. *Phys. Rev. B* **65**, 132514 (2002).
- Laiho, R., Lähderanta, E., Sonin, E. B. & Traito, K. B. Penetration of vortices into the ferromagnet/type-II superconductor bilayer. *Phys. Rev. B* **67**, 144522 (2003).
- Gu, J. Y. *et al.* Magnetization-orientation dependence of the superconducting transition temperature in the ferromagnet-superconductor-ferromagnet system: CuNi/Nb/CuNi. *Phys. Rev. Lett.* **89**, 267001 (2002).
- Golubović, D. S., Pogosov, W. V., Morelle, M. & Moshchalkov, V. V. Little-Parks effect in a superconductor loop with a magnetic dot. *Phys. Rev. B* **68**, 172503 (2003).
- Golubović, D. S., Pogosov, W. V., Morelle, M. & Moshchalkov, V. V. Nucleation of superconductivity in an Al mesoscopic disk with magnetic dot. *Appl. Phys. Lett.* **83**, 1593–1595 (2003).
- Lange, M., Van Bael, M. J., Bruynseraede, Y. & Moshchalkov, V. V. Nanoengineered magnetic-field-induced superconductivity. *Phys. Rev. Lett.* **90**, 197006 (2003).
- Lange, M., Van Bael, M. J., Moshchalkov, V. V. & Bruynseraede, Y. Phase diagram of a superconductor/ferromagnet bilayer. *Phys. Rev. B* **68**, 174522 (2003).
- Tachiki, M., Kotani, A., Matsumoto, H. & Umezawa, H. Superconducting Bloch-wall in ferromagnetic superconductors. *Solid State Commun.* **32**, 599–602 (1979).
- Wadas, A., Rice, P. & Moreland, J. Recent results in magnetic force microscopy. *Appl. Phys. A* **59**, 63–67 (1994).
- Hubert, A. & Schäfer, R. *Magnetic Domains*, 401–410 (Springer, Berlin/Heidelberg, 1998).
- Goodenough, J. B. Interpretation of domain patterns recently found in BiMn and SiFe alloys. *Phys. Rev.* **102**, 356–365 (1956).
- Zhang, X. X., Hernández, J. M., Tejada, J., Solé, R. & Ruiz, X. Magnetic properties and domain-wall motion in single-crystal BaFe_{10.2}Sn_{0.74}Co_{0.06}O₁₉. *Phys. Rev. B* **53**, 3336–3340 (1996).

Acknowledgements

This work is supported by the K. U. Leuven Research Fund GOA/2004/02, Flemish FWO, Belgian IUAP Projects, Bilateral Flanders-China Project BIL 00/02 and the ESF VORTEX Programme. M.L. is a postdoctoral research fellow of the F.W.O.-Vlaanderen.

Correspondence and requests for materials should be addressed to V.V.M.

Competing financial interests

The authors declare that they have no competing financial interests.